

# Effect of $Y_2O_3$ content on the mechanical and optical properties of zirconia-based dental ceramics

A. M. S. Monção<sup>1</sup>, E. M. B. dos Santos<sup>1</sup>, P. L. Gomes<sup>1</sup>, J. E. V. Amarante<sup>2</sup>, B. X. de Freitas<sup>3</sup>, C. Santos<sup>1,4\*</sup>

<sup>1</sup>Universidade Federal Fluminense, Escola de Engenharia Industrial Metalúrgica de Volta Redonda, 27276-210, Volta Redonda, RJ, Brazil

<sup>2</sup>Universidade Federal Fluminense, Faculdade de Odontologia, Instituto de Saúde de Nova Friburgo Dr. Silvio Henrique Braune, 28625-650, Nova Friburgo, RJ, Brazil

<sup>3</sup>Universidade Federal de Itajubá, 37500-903, Itajubá, MG, Brazil

<sup>4</sup>Universidade do Estado do Rio de Janeiro, Faculdade de Tecnologia, 27537-000, Resende, RJ, Brazil

## Abstract

The present work aims to identify variations in the mechanical and optical properties of samples produced from  $ZrO_2$  powders containing different  $Y_2O_3$  contents (3Y-TZP, 4Y-PSZ, and 5Y-PSZ) intended for applications such as dental prostheses. Disc-shaped samples ( $n=60$ ) were uniaxially pressed, sintered at 1550 °C-2 h, and characterized. Dense ceramics were obtained for all compositions. The increase of  $Y_2O_3$  content led to the increase of the cubic- $ZrO_2$  phase with a reducing tetragonal phase. As a result, mechanical properties were reduced (flexural strength of 1375~590 MPa and fracture toughness 7.2~4.1  $MPa \cdot m^{1/2}$ ) while translucency was improved. Based on the requirements of ISO-6872 standard, 3Y-TZP presents versatility for non-aesthetic applications, while 5Y-PSZ is recommended for aesthetic applications such as anterior teeth due to better translucency.

**Keywords:** ceramics, yttria-doped zirconia, mechanical properties, opacity, ISO-6872.

## INTRODUCTION

Among the materials used for dental restorations, zirconia ( $ZrO_2$ ) in its various compositions, shows great potential for use, due to its excellent mechanical and optical properties, especially zirconia doped with yttria ( $Y_2O_3$ ) contents ranging from 3 to 5 mol% [1-4]. In its first generation, tetragonal polycrystalline zirconia doped with 3 mol%  $Y_2O_3$ , also called 3Y-TZP, was applied in dentistry and orthopedics, since such material has a Vickers hardness of around 1200 HV, fracture toughness reaching values between 6 and 8  $MPa \cdot m^{1/2}$  and flexural strength greater than 1000 MPa, with modulus of elasticity in the range of 200 GPa, in addition to being aesthetically whitish in color and presenting high opacity [5-9]. These properties are the result, among other factors, of the toughening phenomenon by phase transformation in zirconia, tetragonal→monoclinic ( $t \rightarrow m$ ), where there is an increase in grain volume and consequent increase in internal stresses, when subjected to high external stresses, resulting in the mitigation of crack growth, thus increasing its fracture toughness.

The second generation of zirconia in dentistry is characterized by a composition like the first generation but with a reduction in the number and size of aluminum oxide ( $Al_2O_3$ ) grains. This modification allowed a greater passage of light and, consequently, a slight improvement

in the partial translucency of the material [10, 11]. However, although suitable for monolithic restorations in posterior teeth, it still did not offer satisfactory aesthetics for use in the anterior region and had a lower translucency when compared to feldspathic or lithium disilicate glass-ceramics [12, 13]. Furthermore, some *in vitro* studies have demonstrated a long-term loss of mechanical strength due to hydrothermal degradation [14-16]. As a result, in the third generation, new ceramic formulations were developed with different proportions of  $Y_2O_3$  (4 and 5 mol% of  $Y_2O_3$ ). These formulations aimed to improve translucency and resistance to hydrothermal degradation compared to 3Y-TZP ceramics while maintaining fundamental mechanical properties for use as a dental material. These ceramics are generally known as partially stabilized zirconia with 4 mol% of  $Y_2O_3$  (4Y-PSZ) and 5 mol%  $Y_2O_3$  (5Y-PSZ) [10, 17, 18].

The 5Y-PSZ ceramics, among the 3 compositions, have the highest translucency, due to the predominant presence of the cubic phase ( $c-ZrO_2$ ) to the detriment of the tetragonal phase, which consequently significantly improves their resistance to hydrothermal degradation. However, this change in composition results in inferior mechanical properties, since the smaller amount of tetragonal phase decreases toughening phenomena, leading to greater brittleness [17, 18]. On the other hand, the 4Y-PSZ ceramics show intermediate mechanical properties and translucency in relation to the two compounds mentioned above. This combination of characteristics makes 4Y-PSZ ceramics suitable for applications in dental prostheses that require

\*[claudineisvr@gmail.com](mailto:claudineisvr@gmail.com)

<https://orcid.org/0000-0002-9398-0639>

good mechanical strength and considerable translucency [19-22]. The objective of this work was to analyze, comparatively, the properties obtained from zirconia with different  $Y_2O_3$  contents, aiming to establish mechanical and optical limits for different clinical dental cases.

## EXPERIMENTAL

Different commercial zirconia ceramic powders were used for this study, including 3Y-TZP (TZ-3YSB-E, Tosoh, Japan), 4Y-PSZ (TZ-PX-630, Tosoh, Japan), and 5Y-PSZ (ZPEX Smile, Tosoh, Japan). The main characteristics of these powders are detailed in Table I. For the characterization of the 3Y-TZP, 4Y-PSZ, and 5Y-PSZ powders, scanning electron microscopy (SEM) and X-ray diffraction (XRD) techniques were used. For phase quantification, Rietveld's refinement technique was used along with crystallographic files of the usual zirconia phases. The details of the procedures used for this characterization are described later.

Samples ( $n=3$ /group) in the form of parallelepipeds measuring  $5 \times 5 \times 20$  mm were individually compacted by uniaxial pressing using a rectangular matrix of  $5 \times 20$  mm base area for each sample group ( $ZrO_2$ -3 mol% $Y_2O_3$ ,  $ZrO_2$ -4 mol% $Y_2O_3$ ,  $ZrO_2$ -5 mol% $Y_2O_3$ ). During compaction, a pressure of 80 MPa was applied for 45 s, and then the samples from each group were separated for thermal analysis by dilatometry. In addition, samples of each composition ( $n=25$ /group) were individually compacted by uniaxial pressing, in the form of discs (thickness of 2 mm and diameter of 15 mm), using the same compaction parameters as previously described. The sintering process was carried out in a furnace with  $MoSi_2$  resistance (ME-1800, Fortelab). The samples were subjected to the following sintering cycle: 1) heating from room temperature to 700 °C, with a heating rate of 1 °C/min, and isothermal time of 60 min; 2) heating from 700 to 1550 °C,

with an isothermal time of 120 min, and a heating rate of 2 °C/min; and 3) controlled cooling with a cooling rate of 5 °C/min to room temperature. After the sintering process, the samples were sanded using diamond sandpaper with grains of 45, 15, and 6  $\mu m$  sequentially, and subsequently polished with diamond suspensions of 3 and 1  $\mu m$  using a polisher (Rotor 2, Knuth). Five samples (sintered ceramic discs) from each group were prepared to reach varied final thicknesses (0.8~2.2 mm) to be analyzed for translucency. Prismatic samples of 3Y-TZP, 4Y-PSZ, and 5Y-PSZ were subjected to dilatometry sintering using a dilatometer (DIL-402C, Netzsch, Germany) under an argon atmosphere with a heating rate of 5 °C/min until reaching a temperature of 1475 °C.

The apparent density of the sintered samples was evaluated by the Archimedes method in distilled water at room temperature, following the ASTM C20-2017 standard [23]. Relative density was estimated by correlating the apparent density obtained with the theoretical density of the samples. The theoretical values of the specific masses were determined using the rule of mixture, considering the specific masses presented in Table I. X-ray diffraction (XRD) analyses were performed on the raw materials and sintered samples using a diffractometer (Empyrean, Malvern PANalytical, UK), which had a  $CuK\alpha$  tube, and the scan was performed in the  $2\theta$  range between 10° and 90°, with an angular step of 0.02 °/s and a scan time of 100 s. Phase identification was carried out using software (X'pert-Highscore, Phillips) and the database in the ICDD files. The morphology of the particles and the microstructure of the sintered samples were evaluated by scanning electron microscopy (SEM, Mira 4-FEG, Tescan). The sintered samples were previously prepared by sanding and subsequent polishing with a 1  $\mu m$  diamond suspension. Then, these polished surfaces were thermally etched at 1400 °C for 15 min and, finally, sputtered with a thin film of gold coating. The SEM micrographs of the samples were obtained at 20 kV to reveal the microstructural characteristics, using the Image-J software.

Nanoindentations were performed on the polished samples using an ultra-microhardness tester (DUH-211S, Shimadzu, Japan), equipped with a Berkovich diamond indenter. Indentation loads ranged from 250 to 1960 mN, and the maximum penetration depth was set to 10  $\mu m$ . The Young modulus (E) of all zirconia ceramics was estimated using the Oliver and Pharr model [24, 25]. The Vickers nanohardness (HV) can be estimated by correlating it with the indentation hardness ( $H_{it}$ ) obtained with the Berkovich indenter:

$$HV = 0.0925.H_{it} \quad (A)$$

where  $H_{it}$  (mN/ $\mu m^2$ ) is the resistance to permanent deformation and can be defined by:

$$H_{it} = \frac{F_{max}}{A_p} \quad (B)$$

Table I - Characteristics of starting powders, according to manufacturer.

| Characteristic                       | 3Y-TZP <sup>a</sup> | 4Y-PSZ <sup>b</sup> | 5Y-PSZ <sup>c</sup> |
|--------------------------------------|---------------------|---------------------|---------------------|
| $Y_2O_3$ (mol%)                      | 3                   | 4                   | 5                   |
| APS ( $\mu m$ )                      | 0.09                | 0.09                | 0.09                |
| $Y_2O_3$ (wt%)                       | 5.2±0.5             | 6.9                 | 7.8                 |
| HfO <sub>2</sub> (wt%)               | <5.0                | -                   | -                   |
| Al <sub>2</sub> O <sub>3</sub> (wt%) | 0.1~0.4             | 0.05                | 0.05                |
| SiO <sub>2</sub> (wt%)               | ≤0.2                | ≤0.02               | ≤0.02               |
| Fe <sub>2</sub> O <sub>3</sub> (wt%) | ≤0.02               | ≤0.01               | ≤0.01               |
| Na <sub>2</sub> O (wt%)              | ≤0.4                | -                   | -                   |
| ZrO <sub>2</sub> (wt%)               |                     | balance             |                     |
| SSA (m <sup>2</sup> /g)              | 7.0±2.0             | 10                  | 10                  |
| Density (g/cm <sup>3</sup> )         | 6.05                | 6.05                | 6.00                |
| MP (°C)                              |                     | 2715                |                     |

<sup>a</sup>: Tosoh Zpex Smile; <sup>b</sup>: Tosoh, TZ-PX-630; <sup>c</sup>: Tosoh, TZ-3YSB-E; APS: average particle size; SSA: specific surface area; MP: melting point.

where  $F_{\max}$  is the maximum force/load and  $A_p$  is the projected contact area, which can be calculated by:

$$A_p = 24.5[h_{\max} - 0.75(h_{\max} - h_r)]^2 \quad (C)$$

where  $h_r$  is the intersection between the loading curve and a tangent line of the maximum force with the horizontal axis in relation to the depth of penetration ( $\mu\text{m}$ ) and  $h_{\max}$  ( $\mu\text{m}$ ) is the maximum depth of indentation. The Young modulus ( $E$ ) was calculated by:

$$E_{it} = \frac{1 - \nu_s^2}{\frac{S\sqrt{\pi}}{2A_p} \frac{1 - \nu_i^2}{E_i}} \quad (D)$$

where  $E=E_{it}$  is dynamic Vickers nanoindentation,  $S$  is the contact stiffness between the indenter and the sample,  $\nu_i$  and  $E_i$  are Poisson's ratio (0.07) and Young modulus (1140 GPa), respectively ( $\nu_s$  is not informed to the user, and was available in the equipment software).

To evaluate fracture toughness, a microhardness tester (HMV-2-Digital, Shimadzu, Japan) with a Vickers indenter coupled with a digital camera was used, applying a load of 9.8 N for 30 s. The indentation method (ASTM C1327-15) [26] was used, performing 25 indentations in each sample. The indentation fracture toughness (IFT),  $K_{IC}$  ( $\text{MPa}\cdot\text{m}^{1/2}$ ), was determined according to Eq. E, valid for Palmqvist crack type (relationship between crack length,  $c$ , and indentation length,  $a$ ,  $c/a < 2.5$ ):

$$K_{IC} = 0.0752 \frac{F}{c^{1.5}} \quad (E)$$

where  $F$  is the applied load (N), and  $c$  is the crack length ( $\mu\text{m}$ ), which corresponds to the distance from the indentation center to the crack tip. Flexural strength was evaluated using a piston-on-3-ball device (P-3B) coupled to a universal testing machine (Emic 1000, Instron, Brazil), with testing performed at a constant speed of 0.5 mm/min until fracture, according to ISO 6872-15 [27]. The dimensions of all specimens were measured with a micrometer and did not vary by more than 0.01 mm between samples. They were wrapped in a thin plastic film to avoid significant friction between the samples and the spheres. The flexural strength,  $\sigma_f$  (MPa), was calculated by:

$$\sigma_f = \frac{0.2387 \cdot F \cdot (X - Y)}{b^2} \quad (F)$$

$$X = (1 + \nu) \ln \left( \frac{r_2}{r_3} \right) + \frac{1 - \nu}{2} \left( \frac{r_2}{r_3} \right)^2 \quad (G)$$

$$X = (1 + \nu) \left[ 1 + \ln \left( \frac{r_1}{r_3} \right) \right] + (1 - \nu) \left( \frac{r_1}{r_3} \right)^2 \quad (H)$$

where  $F$  is the breaking load (N),  $b$  is the thickness ( $1.25 \pm 0.10$  mm),

$r_1$  is the support circle radius ( $r_1 = 5.5$  mm),  $r_2$  is the piston radius ( $r_2 = 0.7$  mm),  $r_3$  is the sample radius ( $6.5 \pm 0.1$  mm), and  $\nu$  is the Poisson's ratio (0.31). Statistical analysis of the evaluation of flexural strength was performed using Weibull statistics [28, 29].

The influence of thickness on translucency (assessed by contrast ratio) of zirconia ceramics was investigated using a reflectance colorimeter (HPS Pro Spectrophotometer, Coralix) following the guidelines established in ISO 2471:2008 standard. Samples with polished surfaces and different thicknesses between 0.8 and 2.2 mm after sintering were used. The spectrophotometer was configured with a light source based on CIE standards for measuring the CIELab color space using the D65 standard. Standard samples were employed to establish white ( $L=99.7$ ,  $a=-0.2$  and  $b=1.5$ ) and black ( $L=22.6$ ,  $a=-0.4$  and  $b=-1.4$ ). The contrast ratio (CR) was obtained as a function of the ratio between the spectral reflectance values, obtained from the luminance measured on the black background and on the white background, according to Eqs. I and J [30-32]. The contrast ratio ranges from 0 (maximum transparency) to 1 (fully opaque).

$$CR = \frac{Y_b}{Y_w} \quad (I)$$

$$Y = \frac{L + 16}{116} \cdot Y_n \quad (J)$$

where  $Y_b$  is the spectral reflectance measured against a black background,  $Y_w$  spectral reflectance measured against a white background,  $L$  luminance, and  $Y_n$  spectral reflectance for light reflected by a perfectly reflected diffuser illuminated by the same light source as the object ( $=100$ ). The translucency parameter (TP) is the color difference of a material on a white or black background. Higher TP values represent higher translucency [30-32]. The translucency parameter was calculated according to:

$$TP = \sqrt{(L_b - L_w)^2 + (a_b - a_w)^2 + (b_b - b_w)^2} \quad (K)$$

where  $L_b$  is the luminance on a black background,  $L_w$  is the luminance on a white background,  $a_b$  is the coordinate  $a^*$  on a black background,  $a_w$  is the coordinate  $a^*$  on a white background,  $b_b$  is the coordinate  $b^*$  on a black background, and  $b_w$  the coordinate  $b^*$  on white background.

## RESULTS AND DISCUSSION

Figs. 1 and 2 show, respectively, the X-ray diffractogram of the raw materials and their respective SEM micrographs revealing the starting powder morphology. The 3Y-TZP powder showed agglomerated morphologies resulting from the binder present in its initial composition. Crystallographic analyses mainly indicated two distinct polymorphs, 90% t-ZrO<sub>2</sub> and

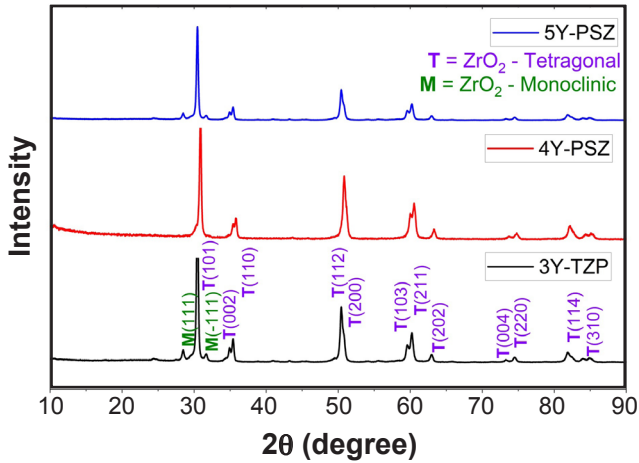


Figure 1: XRD patterns of starting powders: 3Y-TZP, 4Y-PSZ, and 5Y-PSZ.

10% m-ZrO<sub>2</sub>. The 4Y-PSZ powder presented mostly a tetragonal phase (t-ZrO<sub>2</sub>), while in the 5Y-PSZ powder, the presence of 94% of t-ZrO<sub>2</sub> and 6% of m-ZrO<sub>2</sub> was observed.

Fig. 3 presents dilatometry results of 3Y-TZP, 4Y-PSZ, and 5Y-PSZ compacts, where the compatibility between the expansion and shrinkage of the different materials was observed and the highest shrinkage rate started in the range between 1000 and 1100 °C. The materials had good sinterability. Ceramic 5Y-PSZ was the material that initiated shrinkage slightly earlier compared to other ceramics. This information is important for applications of these materials as pre-sintered products, where shrinkage rates are important so that it is possible to estimate the final dimensions of prototypes considering the shrinkage that will occur at a certain sintering temperature, aiming at the manufacture of ceramic prostheses manufactured by CAD/CAM systems. The 3Y-TZP, 4Y-PSZ, and 5Y-PSZ samples reached a relative density of 99.87±0.03%, 99.85±0.06%, and 99.94±0.06%, respectively. Due to the similarity in the densities found between the samples, it was considered that all reached approximately 99.9% of final densification. The dispersion of the individual apparent density values of the sintered samples and the

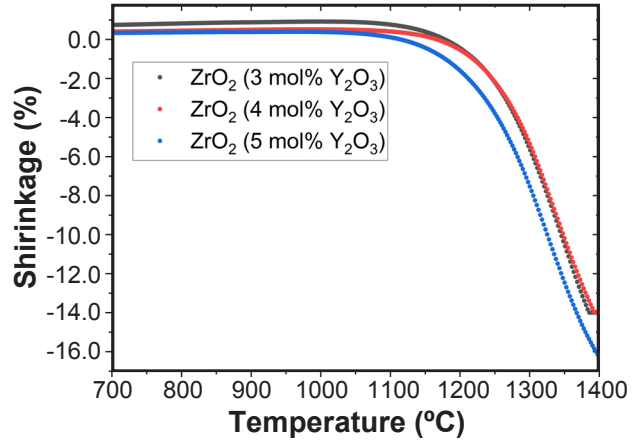


Figure 3: Dilatometry curves of 3Y-TZP, 4Y-PSZ, and 5Y-PSZ powder compacts.

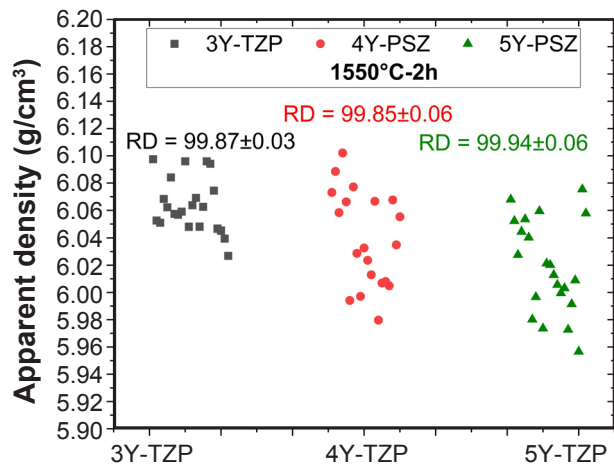


Figure 4: Apparent density with an indication of relative density (RD) of 3Y-TZP, 4Y-PSZ, and 5Y-PSZ samples sintered at 1550 °C-2 h.

average of the relative densities is shown in Fig. 4.

Fig. 5 presents the X-ray diffractograms of the sintered samples and Table II summarizes the characteristics of the phases found and their quantification by the Rietveld method. For the 3Y-TZP samples, three main polymorphs

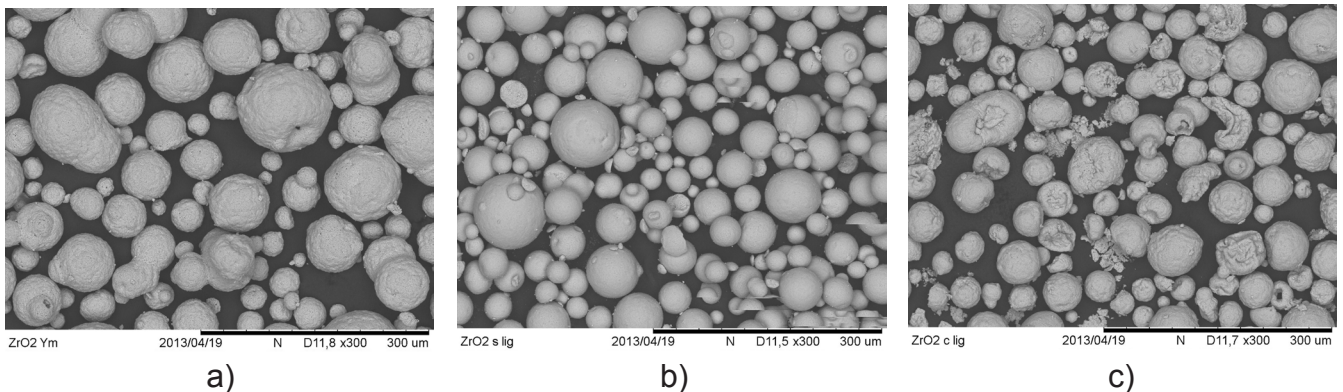


Figure 2: SEM images of spray-dried granules of the starting powders: a) 3Y-TZP; b) 4Y-PSZ; and c) 5Y-PSZ.

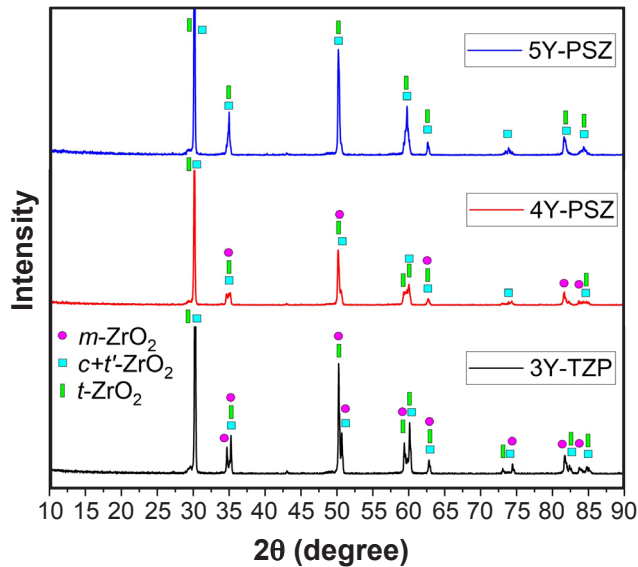


Figure 5: X-ray diffractograms of zirconia samples with 3, 4, and 5 mol% yttria sintered at 1550 °C-2 h.

were identified, with the following proportions: 68.1% t-ZrO<sub>2</sub>, 29.2% c+t'-ZrO<sub>2</sub>, and 2.7% residual m-ZrO<sub>2</sub>. In the 4Y-TZP samples sintered at 1550 °C-2 h, three polymorphs were also observed, with the following contents: 39.7% t-ZrO<sub>2</sub>, 58.7% c+t'-ZrO<sub>2</sub> and 1.6% m-ZrO<sub>2</sub> residual. These samples showed more balanced values between the cubic phase and the others. Finally, in the samples

sintered at 1550 °C-2 h of 5Y-PSZ, two main polymorphs were identified, with the proportions of 81.3% c+t'-ZrO<sub>2</sub> and 18.7% t-ZrO<sub>2</sub>. This last sample exhibited the highest cubic phase values and the lowest amount of toughening tetragonal phase. Since the pseudo-cubic phase (t') behaves very similarly to the cubic (c), they are sometimes considered as a single phase, so here they are together [6]. It was noted that characteristic peaks of the monoclinic and tetragonal phases were more present and intense in the 3Y-TZP sample, such peaks suffered a reduction in intensity in the 4Y-PSZ and a slight increase in the regions related to the cubic (and/or pseudo-cubic) phase. In 5Y-PSZ, the predominance of the cubic phase was evidenced, with traces of tetragonal and the absence of the monoclinic phase, thus corroborating the quantification of Rietveld refinement. In Table II, chi-square ( $\chi^2$ ) is a statistical test that evaluates the goodness of fit of analyzed data.

In Fig. 6, the SEM micrographs of the different zirconia studied in this work (3Y-TZP, 4Y-PSZ, or 5Y-PSZ) are displayed. As a result, Fig. 7 shows the grain size distribution of each sample group. It was observed that the samples from the 3Y-TZP and 4Y-PSZ groups exhibited a heterogeneous granulometric distribution, composed of a matrix of ZrO<sub>2</sub> grains smaller than 1  $\mu\text{m}$ , with the presence of a few grains between 1 and 2  $\mu\text{m}$  and in greater incidence in the 4Y-PSZ. On the other hand, 5Y-PSZ exhibited a bimodal distribution that was also heterogeneous, but with visibly larger grain sizes, ranging from 1 to 5  $\mu\text{m}$ .

Table II - Crystallographic parameters of samples with different Y<sub>2</sub>O<sub>3</sub> contents sintered at 1550 °C-2 h.

| Parameter   | 3Y-TZP                      | 4Y-PSZ                      | 5Y-PSZ                      |
|---|-----------------------------|-----------------------------|-----------------------------|
| ZrO <sub>2</sub> monoclinic (m-ZrO <sub>2</sub> )<br>space group P1 21/c 1                  | a=5.1209 Å                  | a=5.1248 Å                  | -                           |
|   | b=5.2718 Å                  | b=5.2798 Å                  | -                           |
|   | c=5.3041 Å                  | c=5.2870 Å                  | -                           |
|   | V=141.49 Å <sup>3</sup>     | V=141.50 Å <sup>3</sup>     | -                           |
| ZrO <sub>2</sub> cubic (c-ZrO <sub>2</sub> )<br>space group Fm-3m                           | -                           | -                           | a=5.1285 Å                  |
|   | -                           | -                           | V=134.89 Å <sup>3</sup>     |
| ZrO <sub>2</sub> tetragonal (t-ZrO <sub>2</sub> )<br>space group P42/nmc                    | a=3.5988 Å                  | a=3.5985 Å                  | a=3.596 Å                   |
|   | c=5.1756 Å                  | c=5.1697 Å                  | c=5.175 Å                   |
|   | V=67.03 Å <sup>3</sup>      | V=66.82 Å <sup>3</sup>      | V=67.05 Å <sup>3</sup>      |
| Tetragonality (c/a√2)   | 1.0169                      | 1.0168                      | 1.0171                      |
| Y <sub>2</sub> O <sub>3</sub> content of t-ZrO <sub>2</sub> (mol%)                          | 1.92                        | 1.96                        | 1.90                        |
| ZrO <sub>2</sub> tetragonal' (t'-ZrO <sub>2</sub> )<br>(yttria rich)<br>space group P42/nmc | a=3.6182 Å                  | a=3.6141 Å                  | a=3.6215 Å                  |
|   | c=5.1437 Å                  | c=5.1395 Å                  | c=5.1414 Å                  |
|   | V=67.33 Å <sup>3</sup>      | V=67.09 Å <sup>3</sup>      | V=67.43 Å <sup>3</sup>      |
|   | Tetragonality (c/a√2)       | 1.0052                      | 1.0046                      |
| Y <sub>2</sub> O <sub>3</sub> content of t'-ZrO <sub>2</sub> (mol%)                         | 5.67                        | 5.53                        | 5.40                        |
| Phase composition (wt%)   | 68.1% t-ZrO <sub>2</sub>    | 39.7% t-ZrO <sub>2</sub>    | 18.7% t-ZrO <sub>2</sub>    |
|   | 29.2% c+t'-ZrO <sub>2</sub> | 58.7% c+t'-ZrO <sub>2</sub> | 81.3% c+t'-ZrO <sub>2</sub> |
|   | 2.7% m-ZrO <sub>2</sub>     | 1.6% m-ZrO <sub>2</sub>     | -                           |
| $\chi^2$  | 2.83                        | 2.85                        | 2.08                        |

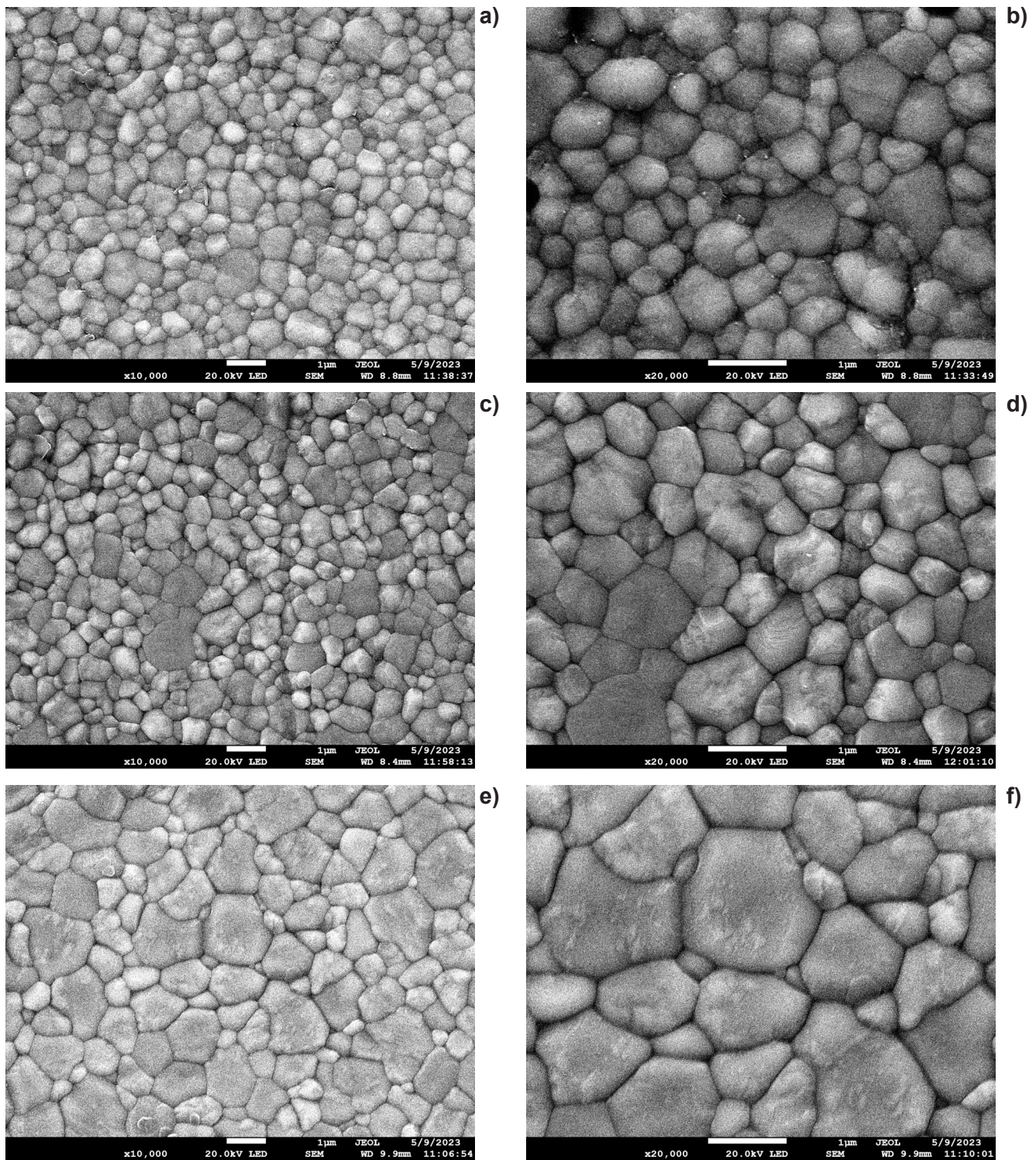


Figure 6: SEM micrographs of the sample sintered at 1550 °C-2 h: a,b) 3Y-TZP; c,d) 4Y-PSZ; and e,f) 5Y-PSZ.

The Vickers hardness and fracture toughness results are shown in Fig. 8. The Vickers hardness and fracture toughness results for the 3Y-TZP sample sintered at 1550 °C-2 h were determined as  $HV=1295\pm34$  and  $K_{IC}=7.2\pm0.2$  MPa.m<sup>1/2</sup>. For the 4Y-PSZ sample, the values obtained were  $HV=1301\pm30$  and  $K_{IC}=5.4\pm0.3$  MPa.m<sup>1/2</sup>. The 5Y-PSZ sample reached the following results:  $HV=1297\pm42$  and  $K_{IC}=4.1\pm0.4$  MPa.m<sup>1/2</sup>. Statistically, the sample groups did not show significant

differences, considering the confidence level of 95%. The technique for determining fracture toughness using Vickers indentation has limitations, but due to its experimental simplicity, it serves as an initial indication of properties. It is suggested that in future work this property be determined by the single-edge V-notched beam method. The Vickers microhardness results found in the literature for the dense zirconia ceramics are of the order of 1300 HV for all 3 types

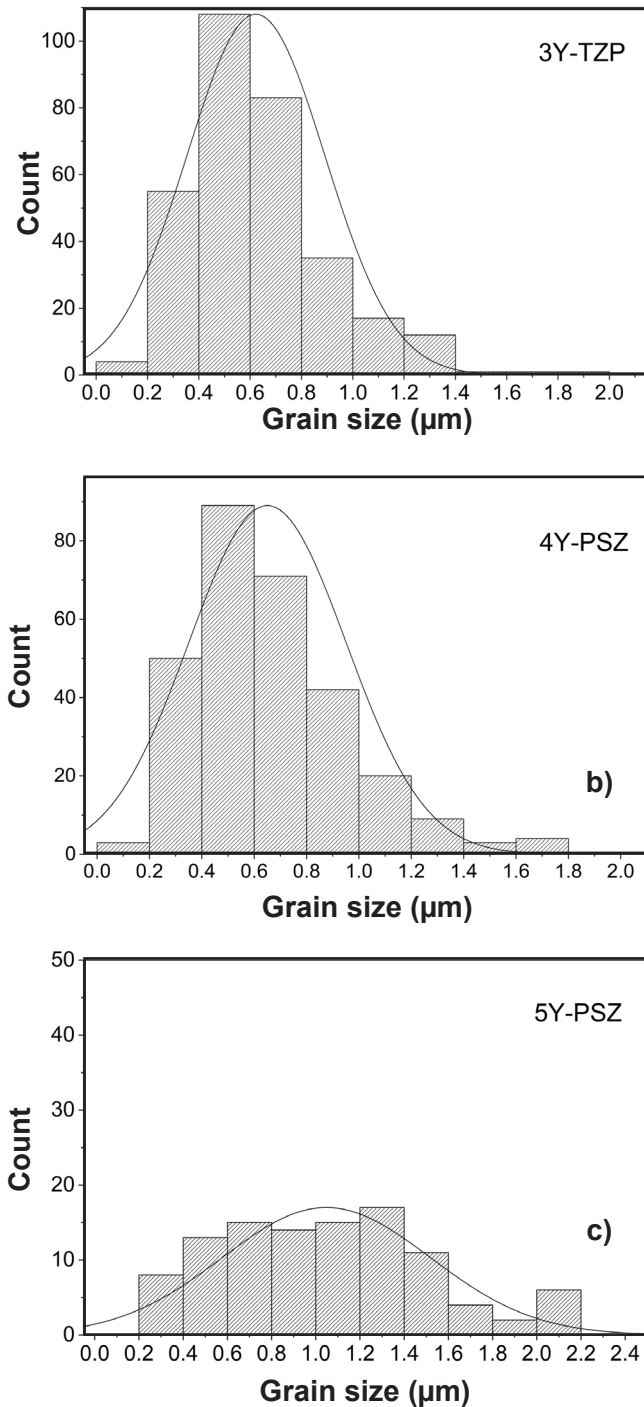


Figure 7: Grain size distribution results of samples sintered at 1550 °C-2 h: a) 3Y-TZP; b) 4Y-PSZ; and c) 5Y-PSZ.

investigated [33]. The fracture toughness values obtained were close to those presented in the literature for monolithic samples of 3Y-TZP, 8~10  $\text{MPa}\cdot\text{m}^{1/2}$ , and other compositions are around 4~6  $\text{MPa}\cdot\text{m}^{1/2}$  [34-38]. This indicated consistency between the results obtained and those reported in the literature.

The results of the nanoindentation measurements and Young modulus as a function of the indentation load, are shown in Figs. 9 and 10, respectively. The nanohardness

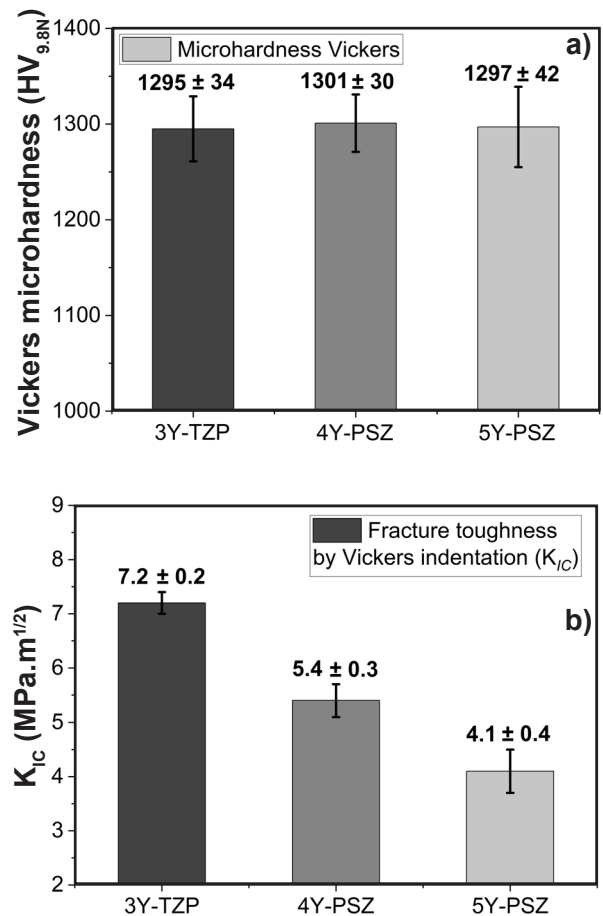


Figure 8: Mechanical properties of the sintered 3Y-TZP, 4Y-PSZ, and 5Y-PSZ samples sintered at 1550 °C-2 h: a) Vickers hardness; and b) fracture toughness.

results for the different materials were similar, regardless of the indentation loads used. In general, the values were in the order of 1550 and 1615 HV. Comparing these results with the results presented in Fig. 8a, an increase in the Vickers hardness values was observed, which may be related to the experimental configuration, which in the case of ceramic materials, indicates that the indentation loads at the nanoscale have a smaller effect of the stress fields around the indentation, which in tests with loads of 1000 gF, therefore, the hardness values increase. In addition, the dispersion of values indicated by the high values of standard deviation indicated that statistically, the three types of ceramics presented similar results for ceramics 3Y-TZP, 4Y-PSZ, and 5Y-PSZ. About the Young modulus, the results presented in Fig. 10 indicate that the ceramics were slightly influenced by the increase in the nanoindentation load. The modulus of elasticity for all ceramics (3Y-TZP, 4Y-PSZ, or 5Y-PSZ) was reduced with an increase in the indentation load (250→1960 mN), as shown in Fig. 10a. As these tests were carried out on a nanometer scale, Fig. 10b shows average values of these measurements shown in Fig. 10a. The results of the Young modulus of the 3Y-TZP, 4Y-PSZ, and 5Y-PSZ ceramics were  $194 \pm 4$ ,  $178 \pm 3$ , and  $213 \pm 3$  GPa, respectively.

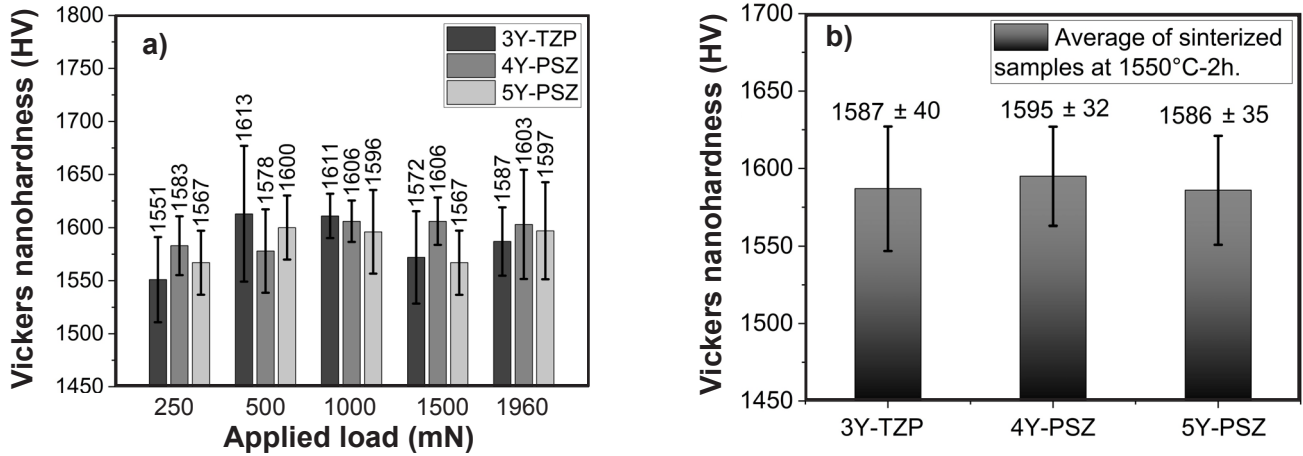


Figure 9: Vickers nanohardness (HV) determined under loads between 250 and 1960 mN (a) and average Vickers nanohardness values (b) of sintered 3Y-TZP, 4Y-PSZ and 5Y-PSZ samples.

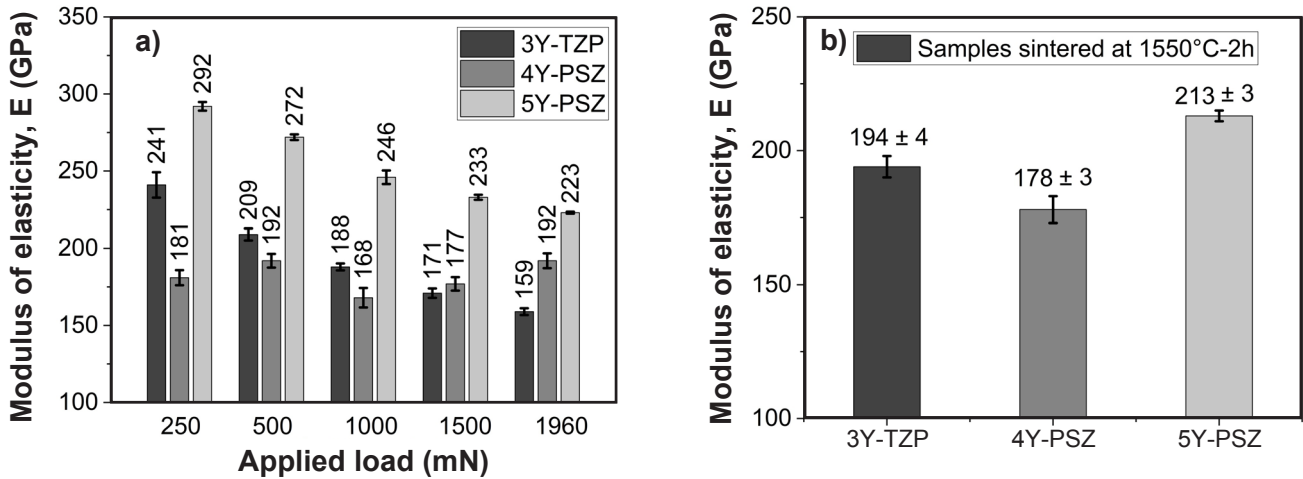


Figure 10: Modulus of elasticity (E) determined under loads between 250 and 1960 mN (a) and average modulus of elasticity (b) of sintered 3Y-TZP, 4Y-PSZ, and 5Y-PSZ samples.

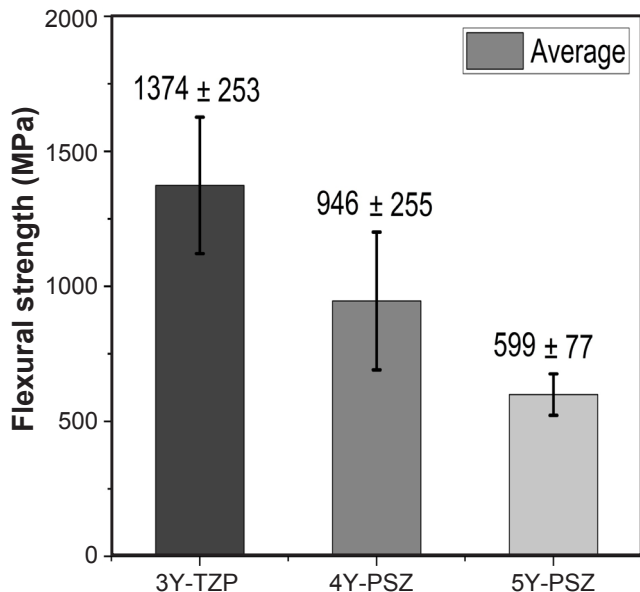


Figure 11: Flexural strength of 3Y-TZP, 4Y-PSZ, and 5Y-PSZ samples sintered at 1550 °C-2 h.

These results were close to the values found for monolithic zirconia ceramics in the literature (200 GPa [39]).

The results of the flexural strength are presented in Fig. 11. Furthermore, Fig. 12 presents Weibull moduli and plots of different zirconia groups. The results presented in Fig. 1 indicate a decrease in flexural strength as a function of the increase of  $Y_2O_3$  doping in different zirconia groups. This lower strength is also linked to greater formation of cubic phase, of lower strength, with increasing yttria content. The average values obtained,  $1374 \pm 253$  MPa for 3Y-TZP,  $946 \pm 255$  MPa for 4Y-PSZ and  $599 \pm 77$  MPa for 5Y-PSZ, were close to and slightly above the values found in the literature for these same materials (900~1100 MPa for 3Y-TZP, 800~1000 MPa for 4Y-PSZ and 400~500 MPa for 5Y-PSZ [39]). The tetragonal phase fraction shown in Table II is closely linked to these results. The larger population of tetragonal-ZrO<sub>2</sub> grains favors the increase of resistance to the crack propagation during P-3B tests since there are mechanical forces in the superficial tetragonal grains, which, when transformed into a monoclinic phase from mechanisms of phase transformation toughening (t→m),

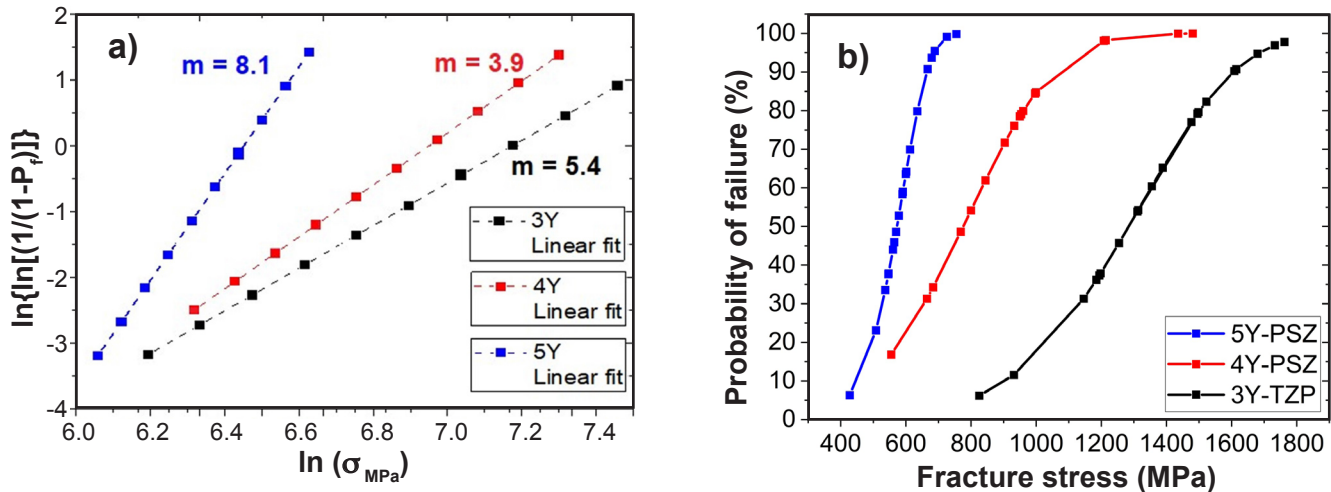


Figure 12: Weibull plots of sintered 3Y-TZP, 4Y-PSZ, and 5Y-PSZ samples with the indication of Weibull modulus (m).

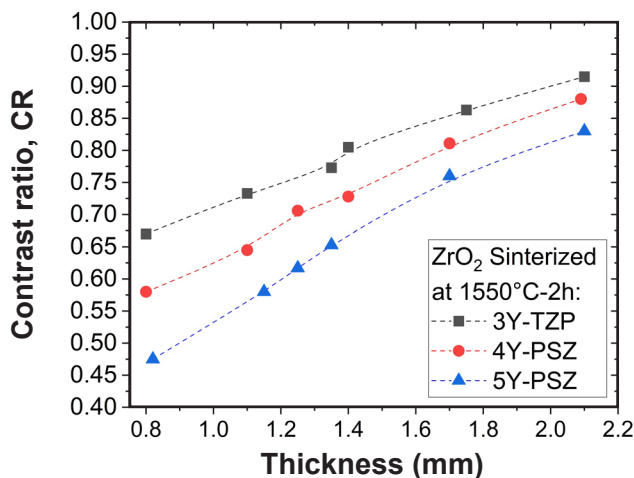


Figure 13: Contrast ratio of sintered 3Y-TZP, 4Y-PSZ, and 5Y-PSZ samples in different thicknesses.

create a shielding zone that increases resistance to crack propagation. As a consequence, the flexural strength of materials with a greater amount of tetragonal ZrO<sub>2</sub> phase is increased. The Weibull moduli (m) obtained for the three different experimental groups were of the order of  $m=5.4$  for 3Y-TZP,  $m=3.9$  (4Y-PSZ), and  $m=8.1$  for 5Y-PSZ resulting in the probability of failure graph shown in Fig. 12 where we can see the highest resistance and consequent lower probability of failure for the 3Y-TZP ceramics, followed by the 4Y-PSZ and having the lowest results for the 5Y-PSZ ceramics, indicating a greater application limitation in areas of high mechanical stress.

The translucency results, represented by the contrast ratio of the samples, can be seen in Fig. 13. It is visible that the 3Y-TZP ceramics had a higher contrast ratio and consequent greater opacity for the same thickness than the 4Y-PSZ and 5Y-PSZ, with the 5Y-PSZ ceramic having the lowest opacity and therefore the highest translucency. This pattern repeated regardless of sample thickness. It should be noted that reducing the thickness of ceramic samples led to an increase

in translucency, regardless of the chemical composition of the zirconia studied. In this sense, a strategy to be considered in the manufacture of a ceramic dental prosthesis is the optimization of these thicknesses, especially of the anterior teeth, which are notably not subject to large chewing forces and require better aesthetic effects.

Among the applications of zirconia-based ceramics in dentistry, especially for dental prostheses, aesthetic effects (here represented by the contrast ratio translucency parameter), and the mechanical requirements of different regions of the dental arch, it is noted that there is a distinction of clinical cases, which are always described by the variation between high translucency when lower mechanical efforts from masticatory loads are required. Therefore, aesthetic tooth prostheses prioritize greater translucency over high mechanical resistance, in these cases, 5Y-PSZ ceramic is the most suitable. In more complex cases, involving the presence of several combined prostheses, involving the presence of molar teeth, responsible for mastication or protocols with 3 or more dental units, the most resistant ceramics, represented here by the 3Y-TZP and 4Y-PSZ ceramics, should be chosen considering, among other aspects, the thickness of the prostheses and smoothing of the dental anatomies to avoid future fracture failures.

## CONCLUSIONS

The different zirconia ceramics containing 3, 4, or 5 mol% Y<sub>2</sub>O<sub>3</sub> achieved complete densification after sintering, with 68% of tetragonal (t-ZrO<sub>2</sub>) and 29% of cubic (c-ZrO<sub>2</sub>) phase contents and residual monoclinic (m-ZrO<sub>2</sub>) phase for the 3Y-TZP ceramics. The increase in the yttria content led to an increase in the cubic phase content and a decrease in the tetragonal phase. Consequently, there was an increase in translucency and a decrease in flexural strength and fracture toughness, as toughening tetragonal ZrO<sub>2</sub> grains were limited. Within the mechanical requirements for the use of zirconia in dentistry, the observed flexural strength values (3Y-TZP 1374 MPa, 4Y-PSZ 946 MPa, and 5Y-PSZ 600

MPa) qualify both materials for use as ceramic prostheses involving molars and highlights the use of 5Y-PSZ ceramics for anterior teeth due to better translucency. However, in mechanically more complex clinical cases, such as multi-element prostheses involving or not molars, the use of zirconia with a higher tetragonal phase content should be sought, therefore, the use of 4Y-PSZ or preferably 3Y-TZP ceramics should be adopted.

## ACKNOWLEDGMENTS

The authors thank FAPERJ (Carlos Chagas Research Support Foundation of the State of Rio de Janeiro) and CNPq (National Council for Scientific and Technological Development) for the financial support given to this project. The authors would like to register a special thanks to Doctoral student Manuel Felipe Rodrigues Pais Alves, for his help in the quantification by the Rietveld refinement.

## REFERENCES

- [1] J. Chevalier, *Biomaterials* **27**, 4 (2006) 535.
- [2] I. Denry, J.R. Kelly, *Dent. Mater.* **24**, 3 (2008) 299.
- [3] A. Bacchi, P.F. Cesar, *Dent. Clin.* **66**, 4 (2022) 591.
- [4] D. Lyon, J. Chevalier, L. Gremillard, *Biomaterials* **20** (2011) 95.
- [5] H. Wang, M.N. Aboushelib, A.J. Feilzer, *Dent. Mater.* **24**, 5 (2008) 633.
- [6] M.F.R.P. Alves, L.Q.B. Campos, B.G. Simba, C.R.M. Silva, K. Strecker, C. Santos, *Ceramics* **5**, 4 (2022) 798.
- [7] B. Basu, *Mater. Rev.* **50**, 4 (2005) 239.
- [8] J. Chevalier, L. Gremillard, A.V. Virkar, D.R. Clarke, *J. Am. Ceram. Soc.* **92** (2009) 1901.
- [9] F. Zhang, M. Inokoshi, M. Batuk, J. Hadermann, I. Naert, B. Van Meerbeek, J. Vleugels, *Dent. Mater.* **32** (2016) 327.
- [10] S. Kreve, A.C. dos Reis, *Rev. Fac. Odont. Porto Alegre* **62**, 1 (2021) 82.
- [11] T. Vagkopoulou, S.O. Koutayas, P. Koidis, J.R. Strub, *Eur. J. Esthet. Dent.* **4**, 2 (2009) 130.
- [12] Y. Zhang, B.R. Lawn, *J. Dent. Res.* **97**, 2 (2018) 140.
- [13] D. Longhini, C.O.M. Rocha, L.T. de Oliveira, N.G. Olenski, E.A. Bonfante, G.L. Adabo, *Oper. Dent.* **44**, 5 (2019) e244.
- [14] Y.R. Fonseca, C.N. Elias, S.N. Monteiro, H.E.S. dos Santos, C. dos Santos, *Materials* **12**, 16 (2019) 2529.
- [15] J.E.V. Amarante, M.V.S. Pereira, G.M. de Souza, M.F.R.P. Alves, B.G. Simba, C. dos Santos, *J. Mech. Behav. Biomed. Mater.* **109** (2020) 103847.
- [16] L.F.O. Lino, E. Bergamo, T.M.B. Campos, E.B.B. Jalkh, A.C.O. Lopes, E.A. Bonfante, *Braz. Oral Res.* **33**, 2 (2019) 1807.
- [17] P.N. Zadeh, N. Lümckemann, B. Sener, M. Eichberger, B. Stawarczyk, *J. Prosthet. Dent.* **120**, 6 (2018) 948.
- [18] L. Mao, M.R. Kaizer, M. Zhao, B. Guo, Y.F. Song, Y. Zhang, *J. Dent. Res.* **97**, 11 (2018) 1222.
- [19] L.V.C. Arcila, N.C. Ramos, T.M.B. Campos, K.S. Dapieve, L.F. Valandro, R.M. Melo, M.A. Bottino, *Dent. Mater.* **38** (2022) e8.
- [20] N.S. Finck, M.I.M. Freitas, M.E.P. de Oliveira, M.G. Bellotti, V.P. Marques, C.F.A. Nobre, *Rev. Eletr. Acervo Saúde* **12**, 11 (2020) e4637.
- [21] C. dos Santos, J. Baltazar, M.F. Alves, S.M. Olhero, *Mater. Lett.* **325** (2022) 132785.
- [22] M.F.R.P. Alves, C. dos Santos, C.N. Elias, J.E.V. Amarante, S. Ribeiro, *J. Biomed. Mater. Res. B Appl. Biomater.* **111**, 1 (2023) 103.
- [23] ASTM C20-17, “Standard test methods for apparent porosity, water absorption, apparent specific gravity, and bulk density of burned refractory brick and shapes by boiling water”, ASTM Int. (2017).
- [24] W.C. Oliver, G.M. Pharr, *J. Mater. Res.* **7** (1992) 1564.
- [25] W.C. Oliver, G.M. Pharr, *J. Mater. Res.* **19** (2004) 3.
- [26] ASTM C1327-15, “Standard test method for Vickers indentation hardness of advanced ceramics”, ASTM Int. (2019).
- [27] ISO 6872, “Dentistry: ceramic materials”, Int. Stand. Org. (2015).
- [28] J.E.V. Amarante, M.V.S. Pereira, G.M. Souza, M.F.R.P. Alves, B.G. Simba, C. Santos, *Mater. Sci. Eng. A* **739** (2019) 149.
- [29] J.B. Quinn, G.D. Quinn, *Dent. Mater.* **26** (2010) 135.
- [30] M.F.R.P. Alves, S. Ribeiro, P.A. Suzuki, K. Strecker, C. Santos, *Mater. Res.* **24**, 2 (2021) e20200402.
- [31] C. Santos, G.O. Rosa, M.N. Quintino, M.F.R.P. Alves, S. Ribeiro, C.L. Melo-Silva, *Ceram. Int.* **46**, 6 (2020) 7748.
- [32] M.F.R.P. Alves, L.G. Abreu, G.G.P. Klippel, C. dos Santos, K. Strecker, *Ceram. Int.* **47**, 1 (2021) 301.
- [33] S.M. Čokić, M. Córdor, J. Vleugels, B. Van Meerbeek, H. Van Oosterwyck, M. Inokoshi, F. Zhang, *Dent. Mater.* **38**, 5 (2022) 797.
- [34] C. Piconi, G. Maccauro, *Biomaterials* **20**, 1 (1999) 1.
- [35] T. Miyazaki, T. Nakamura, H. Matsumura, S. Ban, T. Kobayashi, *J. Prosthodont. Res.* **57**, 4 (2013) 236.
- [36] B.C. Spies, F. Zhang, C. Wesemann, M. Li, *Dent. Mater.* **36** (2020) e329.
- [37] F. Zhang, B. Van Meerbeek, J. Vleugels, *Dent. Mater.* **36**, 4 (2020) 491.
- [38] Y. Yin, J. Xu, M. Ji, L. Li, M. Chen, *Ceram. Int.* **49**, 2 (2023) 1549.
- [39] Y. Zhang, B.R. Lawn, *J. Dent. Res.* **97**, 2 (2018) 140. (Rec. 10/07/2023, Rev. 24/09/2023, Ac. 19/10/2023)

